Catalytic and Non-Catalytic Pyrolysis of Rice Husk Biomass: Kinetic and Thermodynamic Analyses Using the Coats-Redfern Method

By

Ali Azfar Zaidi

School of Chemical and Materials Engineering

National University of Science and Technology

2022

Catalytic and Non-Catalytic Pyrolysis of Rice Husk Biomass: Kinetic and Thermodynamic Analyses Using the Coats-Redfern Method

Name: Ali Azfar Zaidi

Registration No: 00000319140

This thesis is submitted as a partial fulfillment of the requirements for the degree of

MS in Chemical Engineering

Supervisor Name: Dr. Salman Raza Naqvi

School of Chemical and Materials Engineering (SCME)

National University of Science and Technology (NUST)

H-12, Islamabad, Pakistan

June, 2022

Dedication

By the grace of Almighty Allah, who is the most Beneficent and the most merciful

This research is dedicated to my parents, who have always been my source of guidance and support.

To my supervisor who shared his knowledge, gave advice, and encouraged me to fulfill my tasks.

And to all my fellows, with whom I worked with and shared good memories.

Acknowledgements

All praises to Almighty Allah, without His will nothing can happen, who favored us with the capacity to think and made us anxious to investigate this entire universe. Incalculable greetings upon the Holy Prophet Hazrat Muhammad (PBUH), the reason for the creation of the universe and wellspring of information and blessing for whole humankind.

From the core of my heart, I am thankful to my research supervisor, Dr. Salman Raza Naqvi for his unwavering technical and moral support and enlightening me with a research vision and pushing me for excellence. His quest for perfection and excellence had been a source of inspiration and driving force. It is his consistent and encouragement that empowered me to achieve the onerous milestone.

I extend my sincere gratitude towards my guidance and committee members: Dr. Iftikhar Ahmad, Dr. Asif Hussain Khoja and Dr. Umair Sikandar for guiding and supporting me in my research course. It would not have been possible without them. I express my gratitude for Dr. Salman Raza Naqvi for sharing his knowledge and experience regarding research work.

I am thankful of my Seniors who shared their knowledge regarding experimental techniques, and they motivated me in this entire research work. Without any doubt, SCME's supporting staff coordinated with me while I was working on different equipment.

I am highly obligated to my Parents and siblings for their never-ending love. Thanks for believing in me, wanting the best for me, and inspiring me to follow my passion. To my friends Arslan Khan and Uzair Abdullah, thank you for your support, advice, and encouragement.

Abstract

The Coats-Redfern method for model-fitting and its correlation coefficients for various models were used to identify the catalytic and non-catalytic pyrolysis of rice husk biomass kinetics by using the thermogravimetric data. The rice husk was mixed with each catalyst (MTES-beta-zeolite, beta-zeolite, commercial beta-zeolite) at a ratio of 1:0.03 by mass. According to the thermogravimetric data, thermal degradation for catalytic and non-catalytic pyrolysis of rice husk biomass occurred at 250 ° C to 550 ° C. Section I (250-360 °C) and Section II (450-550 °C) of thermal degradation were identified, and the best acceptable models for the behavior of catalytic and non-catalytic biomass pyrolysis were found. All reaction models, including diffusion-controlled reaction, chemical reaction, power-law model, Avrami Erofeev equation, and phase boundary, were kinetically characterized, and they described the nature of biomass pyrolysis. From the activation energy trends, it can be understood that MTES beta-zeolite has no significant effect on pyrolysis in Section I but has significant effects in Section II. The beta-zeolite and commercial beta-zeolite gave better results for all reaction models in both sections by lowering the activation energies for catalytic pyrolysis of rice husk biomass compared to those for non-catalytic pyrolysis. Kinetic analysis of reaction models F1, F1.5, D2, D3, and D4 described appropriate results that are in approximation with each other for both sections.

Table of Contents

List of Figures

List of Tables

Acronyms

BET: Brunauer-Emmett-Teller

DTG: Differential thermogravimetric analysis

DGC: Dry gel conversion

FTIR: Fourier transform infrared spectroscopy

GHG: Greenhouse gas

MTES: Methyltriethoxysilane

TEAOH: Tetraethylammonium hydroxide

TEM: Transmission electron microscopy

TGA: Thermogravimetric analysis

TPD: Temperature programmed desorption

XRD: X-rays diffraction

Chapter 1

1 Introduction

1.1 Background

Biomass is one of the most proven renewable energy sources in the replacement of other fuels because of its abundance and recovery of a variety of products. Rapid economic development, industrial growth, and urbanization increased greenhouse gas (GHG) emissions, posing new challenges for limiting global warming to 1.5 ℃ [1]. These negative consequences of using fossil fuels as primary energy resources are drawing attention to their mitigation and consideration of eco-friendly alternatives to help the ecosystem remain green. Recent research in the fields of energy and the environment is focused on limiting CO_2 emissions by replacing fossil fuels with cleaner alternatives to energy production [2]. Lignocellulosic biomass, such as rice husk, is one of the main agricultural crops that are cultivated in many Asian countries including China, Vietnam, India and Malaysia [3].

1.2 Rice Husk a potential biomass

Rice husk has been proved a potential biomass as a source of clean energy production due to abundant production of rice, worldwide [4]. Despite its vast production around the world of approximately 134 MT/year, 90 % of rice husk biomass is disposed in open channels or burned openly, leading to an increase in GHG emissions [5]. Rice husk has been shown to be the second crop residue in the Sindh and Punjab provinces of Pakistan, which is why it is considered potentially attractive biomass due to its high availability and low cost. Pakistan Alternative Energy Board's, in conjunction with the World Bank assessment, 25 rice mills are in these two provinces, corresponding to rice husk production and energy generation, [3, 5-7]. In the Figure 1 the whole process of rice husk production is welly described by categorizing into best possible resources.

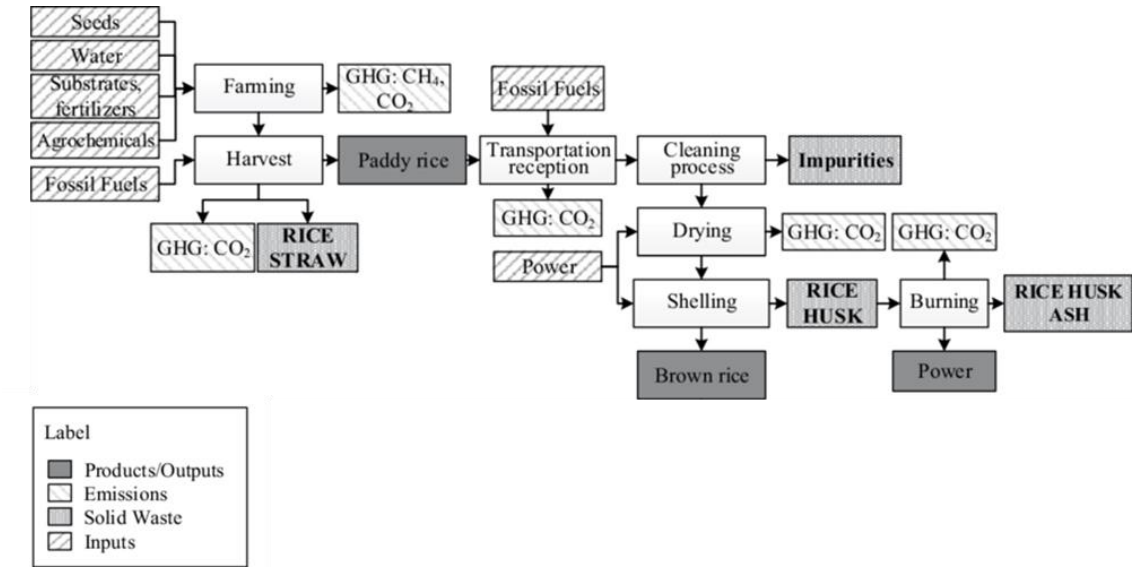

Figure 1 Rice husk production process by categorizing into four major labelled resources

The conversion of rice husk to bioproducts can be valorized through thermochemical conversions and recovery of the desired products. Biomass thermochemical conversions such as combustion, liquefaction, gasification, carbonization, and pyrolysis lead to the production of value-added biofuels (solid, liquid, and gas), which have many applications compared to conventional fuels [8]. Each thermochemical process has its different socio-economic and technological perspectives, which have recently been addressed and reviewed [9]. Among these potential thermochemical processes, recent efforts have concluded that the versatile and intricate pyrolysis process involves overlapping reactions and intermediate products [9].

1.3 Pyrolysis of Rice Husk

Pyrolysis is a procedure of altering diverse form of RH in absence of oxygen to generate various categories of product based on their nature. In the pyrolysis process, organic compounds are converted into valuable products likely, solid (chars), liquid (Bio-oil) and volatile gas (Bio-gas) by heating them at elevated temperatures in the absence of oxygen

or an inert environment. The distribution of pyrolysis products varies with feedstocks and heating rates and can be used in industries as an energy resource or chemicals (biogas, bio-oil, and char) [6, 10-13]. Studies have shown that conventional pyrolysis produces unwanted byproducts, such as tar and char, along with desired products, such as syngas [15]. These by-products promote the formation of coke and block the pores of the filters, which is troublesome [3]. The addition of a suitable catalyst to the pyrolysis process can enhance efficiency by increasing syngas yield and compensating for tar products [4, 14-16].

1.3.1 Mechanism of Pyrolysis

Pyrolysis process starts with the formation of vapors of volatiles, then it destined into valuable products (Biofuel, petrochemicals etc.) by the deprivation of non-volatiles. Then with the increasing temperature hydrocarbons and benzene derivatives in the gaseous form are produced by the secondary decomposition of char. A schematic demonstration of RH pyrolysis mechanism is given in Figure 2. With the temperature increase, the fuel gas having higher percentage of hydrogen produces because dehydrogenation reactions de-carbonization of oxygenated hydrocarbons can increase in H2 content that comes from substantial hydrocarbon compounds. Furthermore, H2 can be act as upright pointer for the secondary cracking of tars to reduce the amount of it.

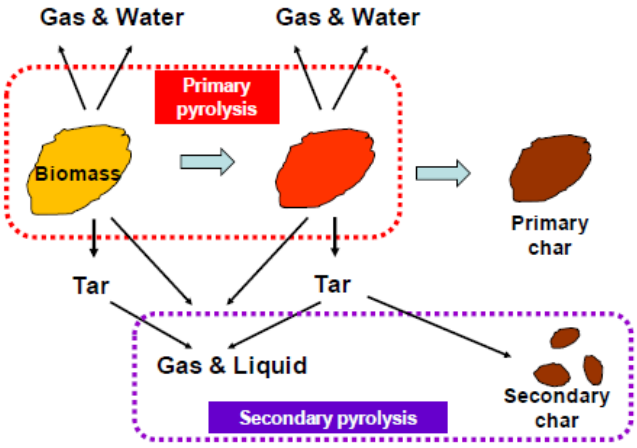

Figure 2 Mechanism of solid degradation reaction in a pyrolysis process.

Menéndez et al. concluded that CO and CO_2 produce at the temperature range of below 450°C due to the breakage of carboxyl and carbony functional groups of RH. CO is the main secondary product produced at elevated temperature due to the cracking reaction. Moreover, hydrocarbons also degrade at high temperatures, that can be illustrated in reaction below:

$C_2H_6 \rightarrow C_2H_4 + H_2$

$C_2H_4 \rightarrow CH_4 + C$

1.3.2 Catalytic pyrolysis

When we loaded the feedstock with some specific species which has an impact on lowering the activation energy during a chemical change or reaction occurs in pyrolysis, then it's associated with catalytic pyrolysis and that foreign species is known as catalyst. In Figure 3 it could be visualized how catalyst influence the activation energy as reaction progress. Catalyst not only favors the extent of happening a reaction at lower temperature but also increase the selectivity of a catalyst.

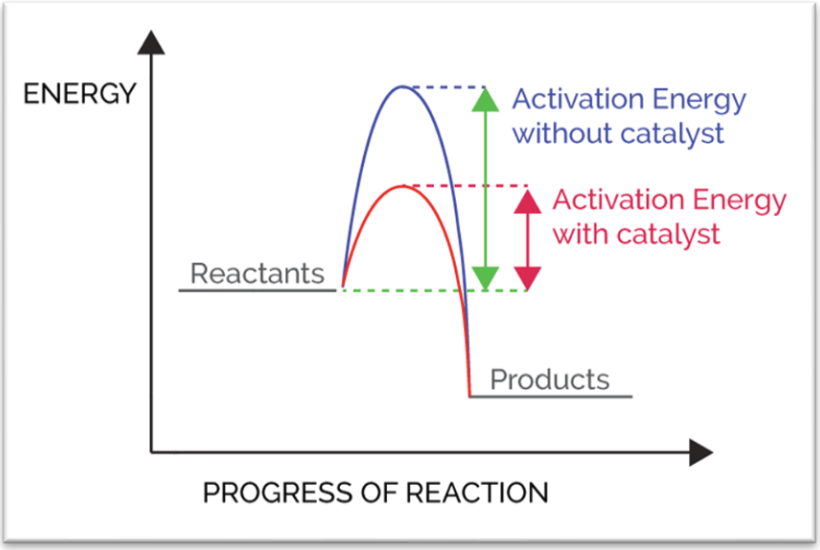

Figure 3 Catalyst impact on Activation Energy

Researchers, recently have a wide scope of study of catalytic processes to make processes greener and products selective. By using specific catalyst, the quality of pyrolysis products can be improved effectively. Pyrolysis products, especially bio-oil can have a various application as a replacement of gasoline and diesel, but due to presence of oxygen in its components it has some limitation. That why oxygen should be eliminated from bio-oil to increase its stability and usage in the replacement of hydrocarbons. For this purpose, two approaches: a) hydrotreating and b) catalytic cracking, has been widely studied. In catalytic pyrolysis process later approach can be easily incorporated by cracking higher complex compounds into products containing less content of oxygen molecules. Through literature survey, zeolites found one of the most efficient products selective catalysts to meeting the requirements at ambient pressure. Bio-oil consist of majorly carboxyl, phenolic, carbonyl compounds and water; all of these compounds are oxygen rich in nature. Bio-oil can be highly upgraded to carbon rich compounds by removing the active oxygenates from it, which can highly influence its stability and coke deposition abilities while applying to thermochemical processes.

1.3.3 Zeolites as a catalyst

Zeolites are aluminosilicates with a compact and well-defined framework and contain alkali and alkaline earth metals. Due to their uniform ordered structure with a pore size <2 nm, zeolites have high thermal and mechanical stability. Their distinctive characteristics include high porosity, hydrophobicity, high specific surface, acidity or basicity of the surface, and resistance to coke deposition and formation [17]. The high shape selectivity feature makes zeolites promising compounds in terms of their application as a catalyst. Many defects in their microporous structures are found, improving their surface properties and making them a widely used catalyst with many applications [11]. The pyrolysis of biomass using zeolites as a catalyst improved the selectivity of desired products, and it captured significant interest in emerging processes[11-13].

1.3.4 Analytical Pyrolysis

Any lignocellulosic biomass thermally degrades in the following hierarchy: moisture elimination, degradation of hemicellulose, degradation of cellulose, and at elevated temperature, finally degradation of lignin occurs [9]. Thermal decomposition of biomass

can be precisely defined by studying kinetic and thermodynamic parameters [10]. The kinetic parameter involves activation energy that is highly depends upon biomass composition and the conditions of the pyrolysis, for example, particle size, catalyst presence, and the temperature of decomposition [12]. Kinetic studies are mainly incorporated by performing a thermogravimetric analyzer [9, 12, 14-16]. In this technique, the investigation of mass loss corresponding to thermal decomposition is done at a specific heating rate. However, catalytic pyrolysis of rice husk biomass using novel boosted defect zeolites as a catalyst has rarely been investigated [14].

The thermogravimetric analyzer (TGA) is generally performed at a constant heating rate, which is described by the mass loss curve versus temperature. In this experiment, the percentage of mass loss is recorded against the temperature. Similarly, the extent of the reaction versus the temperature can easily be obtained. For kinetic analysis, it adopts the integral analysis method for the validation of the reaction conversion curve. Two methods are usually considered for the kinetics study: a) the model-free method and b) the model-fitting method. For the single heating rates model fitting method is usually applied and for multiple heating rates model free method is considered the best technique [18, 19]. That's why integral method-fitting of the Coats-Redfern model was adapted to comprehensively describe the kinetic parameters [16] in this work.

1.4 Problem Statement

Rice husk has been proved a potential biomass as a source of clean energy production due to abundant production of rice, worldwide. Combustion was considered only way to make recover energy from rice husk, though leading to an increase in GHG emissions [5]. Nowadays, thermochemical process like pyrolysis is being employed to convert rice husk into different valuable products but their quality needs many improvements for their usage. These bio-products contains aldehyde, ketones, carboxylic acids, carbonyl, and phenolic compounds, which have much oxygen contents in it. These products of conventional pyrolysis are not stable in terms of their usage and replacement to the hydrocarbon fuels like gasoline, diesel etc. These gaps are still to be addressed and there

is a need to improve the bio-products quality by employing a suitable catalyst which could have lower the oxygenates and significant effects on kinetic and thermodynamic parameters. Pyrolysis of rice husk using defects boosted zeolites as a catalyst is one of the considerable ways to address this hotspot.

To demonstrate the zeolite catalysts effects on rice husk pyrolysis the detailed approximation of kinetic and thermodynamic parameters is vital for considerate and modelling of pyrolysis process at commercial scale. So, this project has comprehended resolution to interpret a detail description of defect boosted zeolite preparation, characterization, and rice husk catalytic pyrolysis kinetic and thermodynamic analysis. The Coats-Redfern method was used by consolidating different models, including reaction order, diffusion-controlled reaction, power law, Avrami-Erofeev equation, and phase boundary mechanisms. The best-fit model was subjected used to study the kinetic results [14-16, 20].

1.5 Research Objective

To address the current challenges in rice husk pyrolysis, this thesis inspects the catalytic and non-catalytic pyrolysis of rice husk. The inclusive research objective is to study the performance of shape modified zeolite catalyst by analyzing the kinetics and thermodynamics by performing TGA. The following assessable objectives are undertaken in the present study.

- To study the rice husk catalytic and non-catalytic pyrolysis behavior by performing thermogravimetric analysis
- To analyze the influence of shape modified beta zeolite catalysts on catalytic pyrolysis by comparing with non-catalytic pyrolysis of rice husk
- To determine the kinetic and thermodynamic parameters of rice husk catalytic and non-catalytic pyrolysis by using the model fitting Coats Redfern method

1.6 Scope of Study

The following scope was established to ensure that the research would be carried out in the time available:

- Pyrolysis of rice husk using shape modified beta zeolites as a catalyst is one of the considerable ways to address the research hotspot.
- To demonstrate the zeolite catalysts effects on rice husk pyrolysis the detailed approximation of kinetic and thermodynamic parameters is vital for considerate and modelling of pyrolysis process at commercial scale. This work has comprehended resolution to interpret a detail description of defect boosted zeolite preparation, characterizations (XRD, TEM, BET, and FTIR), and rice husk catalytic pyrolysis kinetic and thermodynamic analysis.
- The Coats-Redfern method was used by consolidating different models, including reaction order, diffusion-controlled reaction, power law, Avrami-Erofeev equation, and phase boundary mechanisms. The best-fit model was subjected used to study the kinetic results.

1.7 Chapter Summary

This manuscript contains of five sections. The contacts of each section are specified in the following passages.

- **Chapter 1** delivers need of proposed topic, contextual and existing issues related to the topic. It also clarifies the definite terms, process, problem statement, objectives, and scope of the strategic research work.
- **Chapter 2** will draft the literature survey accomplished to describe preceding efforts done on the zeolites employed as a catalyst and their effects of biofuels production obtained from various sources.
- **Chapter 3** contains the methodology associated to the sample preparation and characterization, pyrolysis inquiry work and kinetic and thermodynamic analysis. It will also provide the related information about procedure and apparatus contributing in the experimental investigations.
- **Chapter 4** delivers results and discussions. The material characterization, experimental, kinetic and thermodynamic modelling consequences are existed and explained based on various point of view.
- **Chapter 5** contains all the findings and conclusions in the existing learning and delivers the upcoming endorsements for the related work.

Chapter 2

2 Literature Survey

2.1 Introduction

Rice husk has been proved a potential biomass as a source of clean energy production due to abundant production of rice, worldwide [4]. Despite its vast production around the world of approximately 134 MT/year, 90 % of rice husk biomass is disposed in open channels or burned openly, leading to an increase in GHG emissions [5]. Rice husk has been shown to be the second crop residue in the Sindh and Punjab provinces of Pakistan, which is why it is considered potentially attractive biomass due to its high availability and low cost. Pakistan Alternative Energy Board's, in conjunction with the World Bank assessment, 25 rice mills are in these two provinces, corresponding to rice husk production and energy generation, [3, 5-7]. In this section the catalyst selection and importance of zeolites is describes as per literature review.

2.2 State-of-the-art Review of Biomass Deoxygenation

Biomass-derived biofuels are difficult to use due to the presence of a higher percentage of oxygen content (more than 35%) compared to fossil-derived fuels [21]. The presence of this high amount of oxygen deteriorates the quality of the products and leads to many technical problems, such as corrosivity, lower viscosity and volatility, acidity, thickening of lubricants, and carbon deposition [22]. Additionally, oxygenated components can be a cause of unnecessary carbon loss, resulting in a reduction in the percentage of oil and energy recovery. Therefore, it is necessary to upgrade or deoxygenate biomass-derived fuels before introducing them into petroleum refineries [23]. Typically, oxygen can be removed in the form of H_2O, CO, and CO_2 following the reaction path of HDO (hydrodeoxygenation), DO (deoxygenation), DCO (decarbonylation) and DCO_2 (decarboxylation), including some parallel reactions such as cracking and isomerization [24]. Deoxygenation typically occurs in the temperature and pressure ranges of 250-450 °C and 1-300 bar, respectively [24]. Breakage of the C-O bond is a complex and difficult

task without catalytic. Therefore, the use of catalysts is an essential step in biomass deoxygenation to assist in the cleavage of the C-O bond and reduce the oxygen content more effectively and efficiently [25].

2.3 Catalytic Deoxygenation Using Zeolites

Catalytic deoxygenation is a feasible method for producing better quality biooils. Hydrodeoxygenation and deoxygenations are the two main reactions in the catalytic deoxygenation process. HDO requires the use of hydrogen gas at high pressures to cleave the C-O bond present in the biooil compounds. Although hydrogen is considered a sustainable energy source, however, since it is a fossil-derived fuel and the main source of CO_2 release, only the DO reaction is considered as a significant route [26]. In the DO route, hydrogen is produced during the water gas shift reaction to facilitate the hydrogenolysis reaction [27]. The only drawback of the DO route is that the final product contains one carbon number less than that of the raw material; however, it is still a better choice compared to HDO.

Numerous catalysts are available that are being successfully utilized in DCO, DCO2, and HDO processes, such as carbon-based catalysts, metallic oxide catalysts, and inorganic additives. However, these catalysts are typically costly, have a risk of pollution associated to SO_x emission, low catalytic acidity, and poor product selectivity[22, 28]. Zeolites with various pore sizes and active sites have proven to be good catalysts to increase biooil yield in DO reactions[14]. Zeolites with different metal supports such as Pb, Cu, Ni, Co, Zn, Al, Fe, Mo, Ti, Ga, and Tn have been used to enhance the catalytic activity and selectivity, especially with metals in the oxide form [29].

Mihalcik et al. studied the catalytic deoxygenation of bagasse, oak, corn cob, and corn stove over different acidic zeolites and showed that among all other catalysts studied, ZSM-5 showed a better result in terms of oxygen reduction and hydrocarbon production to produce a more stable biooil[30].Experimented to check the selectivity and yield of liquid oil on aluminum-supported zeolites and predicted that H-Beta provides high selectivity and H-ZSM-5 gives a higher percentage of aromatic compounds. It is

investigated the influence of metal-modified zeolites with three different metals, Fe, Co, and Zr, on sawdust-derived pyrolytic oil. They suggested that iron- and zirconium-based ZSM-5 catalysts promote the formation of aromatic hydrocarbons; however, cobalt-based ZSM-5 promotes more gas yield and coke formation.

2.3.1 Role of Catalyst Pore Size and Shape

Zeolites are nano porous, crystalline, aluminosilicate materials. Nanopores can be further classified into mesoporous or microporous on the basis of molecular dimensions. Due to the uniform pore size, structure, stability, geometry, and strong acidity of zeolites, they have been effectively used in the catalytic deoxygenation of different biomass-derived biooils. Lewis and Bronsted acidity, high specific surface area, adsorption capacity, stability, and specific shape make zeolites an excellent catalyst in many petrochemical and refinery operations.

Zeolite can be synthesized using different techniques, such as thermal ionic, xerogel, vapor phase, solvothermal, hydrothermal synthesis, and doping. For example, X, Y, and Beta zeolites have slightly large micropores (20-500), consisting of 12-membered rings. The benefit of these large pores is that the catalyst is easily accessible, but it can also cause pore blockage and coke deposition due to the participation of more molecular intermediates during polymerization. ZSM-5 has a 3D system with 10-membered rings and a pore size range of 5.2 to 5.5Å. These tiny pores restrict unwanted reactions and aid desirable reactions such as aromatization and alkylation.

Naqvi et al. studied the oil upgradation obtained from pyrolysis paddy husk in a fixed-bed reactor under the catalytic activity of 10-membrane ring zeolites and predicted that ZSM-5, with 1152.32µmol/g active acidic sites, showed the highest organic yield in pyrolytic oil, compared to the other catalysts in the study. Rownaghi et al. suggested in their study that a single mesoporous unit of zeolite catalyst has a large surface area and pore volume compared to a typical simple ZSM-5, especially in the deoxygenation of methanol. Wang et al. investigated the effect of the ZSM-5 catalyst on lignin conversion into phenols and

explored that the nano porous catalyst showed higher phenol conversion, lower coke formation, and stronger activity compared to the microporous ZSM-5 catalyst.

2.3.2 Zeolite Application in Pyrolysis Oil Generation

The hydrated silicoaluminate compounds, zeolites, are crystalline structures formed by interlinked tetrahedral silicate and aluminate compounds. Owing to the open cavities and crystalline nature of zeolites, they undergo changes during pyrolysis reactions. The porosity, availability of active sites, and acid content can enhance not only the deoxygenation of reactants but also the aromatic yield of the pyrolysis product. Several studies have been conducted and reported on the use of zeolites as catalysts for biomass pyrolysis with promising results. Zeolites as catalysts can be used to significantly enhance the pyrolysis of biomass into biooils and biofuels. The development of a highly efficient and stable catalyst for the production of biofuels from biomass is a challenge. High-quality biooil can be obtained by cracking, aromatizing, ketonizing, and condensation. Aderibigbe et al. reviewed the catalysis of pyrolysis through recently developed zeolites, which involve hydrogenation and improved hydrodeoxygenation conversion of pyrolysis oil to aromatics and other valuable chemicals.

Binnal et al. reported the pyrolysis of rice husks through the Zeolite Socony Mobil-5 catalyst (ZSM-5) at 400-600 ° C. When the pyrolytic temperature was increased, the pyrolysis was increased, thereby increasing the polycyclic aromatic hydrocarbon content in biooil. Only the appropriate pyrolytic temperature resulted in the production of biooil because at low temperature, the biooil was converted into water and gases at high pyrolytic temperature. Similar results were obtained using iron-modified protons and zeolites as heterogeneous catalysts. Aho et al. reported the pyrolysis of pine wood with acidic zeolite at 450 °C. The yield of biooils changed as a result of an alteration in the zeolite structure, while their chemical composition is also affected by the zeolite structure. Modified ZSM-5 catalysts, such as hydrogen-exchanged ZSM-5 (HZSM-5) have been found to catalyze the pyrolysis of microalgal biomass. In addition, high-HV biooil can be obtained by using plastic waste via fast pyrolysis. However, the uncatalyzed pyrolysis of biomass yields biooils with long carbon chain compounds. Thus, the catalytic pyrolysis facilitates the

high yield of biooils aided by aromatic hydrocarbons. Variations in the physicochemical properties and composition of biooils obtained by pyrolysis make them attractive as renewable and green energy resources. The zeolites as catalyst also exhibit a positive effect on the production of biogas during pyrolysis at low temperature, and the synthesized biogas is rich in C_3-C_4.

Furthermore, secondary cracking can also be controlled with modified Ce-loaded HZMS-5 for the synthesis of pyrolysis oil. Recently, high-quality biofuels have been synthesized using activated carbons derived from activated carbons derived from renewable biomass. Mullen and coworkers reported microwave-assisted cellulose pyrolysis for enhanced phenol selectivity. Zeolites can be used to improve the yield of pyrolysis oil. HZSM-5 zeolites are highly efficient in removing oxygen from oxygenated compounds. Several studies reported the high yield of biooils by using zeolites or modified zeolites.

Zeolites can be combined with metals to enhance their catalytic efficiency as a heterogeneous catalyst. A modified zeolite, such as Co-Zn/HZSM-5, can not only increase the yield of hydrocarbons but also decrease the yield of oxygenated compounds. Another zeolite, Pd/HZSM-5 @ mesoSiO2, can be synthesized by combining the catalyst at 3:1 of synthesized Pd and tetraethyl orthosilicate/HZSM-5, for improved biomass pyrolysis oil yield by biomass [23]. Cheng et al. studied the effect of HZSM-5 catalysts at different Ni concentrations and evaluated the role of the Zn/HZSM-5 catalyst in biomass pyrolysis. Furthermore, they reported that Zn/HZSM-5 exhibited a higher catalytic efficiency and produced more hydrocarbons than HZSM-5 alone. Although carbonaceous biomass can be easily deposited on a zeolite surface by pyrolysis, its topology and acidic properties affect the concentration and nature of the product. The degree of coke formation during biomass pyrolysis also depends on the properties of the zeolites. The zeolites are also highly selective and thus can be easily deactivated. During the upgradation of pyrolysis oil, zeolites in variable proportions affect the production of coke deposits and the potential for catalyst activation. The behavior of the catalyst can be evaluated in terms of the production of biofuels along with the reduction of coke.

2.3.3 Shape Modified Beta Zeolites

Beta Zeolites are nano porous, crystalline, aluminosilicate materials. Nanopores can be further classified into mesoporous or microporous based on molecular dimensions. Due to the uniform pore size, structure, stability, geometry, and strong acidity of zeolites, they have been effectively used in the catalytic deoxygenation of different biomass-derived bio-oils and Bronsted acidity, high specific surface area, adsorption capacity, stability, and specific shape make zeolites an excellent catalyst in many petrochemical and refinery operations[31-33]. Zeolites have promising results on the catalytic pyrolysis of rice husk, which were concluded in [12, 31, 34-37]. The catalytic pyrolysis of biomass using defect-boosted zeolites as a catalyst has not yet been investigated. Defect-boosted zeolites have significant effects on the cracking of low density polyethene as well described in [11].Thus, this work investigated kinetic and thermodynamic parameters by tailoring different reaction models. Our ultimate focus is to investigate the effects of a high-structural defected catalyst on the kinetic parameters. In catalytic pyrolysis, we used MTES beta H-type having silanol group, beta H-type, and Commercial beta H-type zeolites which have an ordered framework, well-defined acid properties, and a porous structure. This study mainly focused on the characterization and analysis of whole rice husk biomass pyrolysis, rather than the individual step and reactions. The Coats-Redfern method was consolidated through different models, including reaction order, diffusion-controlled reaction, power law, Avrami-Erofeev equation, and phase boundary models. The best-fit model will be used to study the kinetic results [14-16, 20].

2.4 Challenges

Pyrolysis oils are complex mixtures that contain up to 300 different compounds and have a high moisture (20 - 30%) and oxygen content. Although zeolite-supported zeolites and metal catalysts have been shown to upgrade biooils. there are still several challenges and hurdles in the application of zeolite-based catalysts for the catalytic deoxygenation of biomass pyrolysis oil. For example, the presence of inorganic residues in biooils can block zeolite micropores, leading to rapid catalyst deactivation [38]. The transport of bulky biooil components and reaction intermediates into and out of zeolites micropores faces

severe limitations in mass transfer limitations [39]. The extent of deoxygenation depends strongly on the nature of the C-O bond, as well as the degree of unsaturation in the oxygenated molecules [40]. The cross-interaction of some compounds in biooil, especially in the presence of acid sites, could also lead to polymerization [41, 42] and result in the plugging of hydrotreatment reactors. Water vapor and oxygenated species promote the sintering and poisoning of active sites of supported metal catalysts. Recovery, regeneration, and reuse of zeolite catalysts at the end of the reaction is also a crucial issue, since repeated reaction regeneration steps often lead to dealumination and loss of acid sites, and hence to irreversible deactivation of zeolites [43, 44]. Furthermore, the cost associated with the use of zeolite-supported noble metal catalysts could be a prohibitive factor for the commercial use of such catalysts [41].

With the challenges associated with the use of zeolite catalysts in the catalytic deoxygenation of biomass pyrolysis oils in mind, the below mentioned recommendations can be predictive for advance research in the field.

(1) Zeolites are shape-selective catalysts; therefore, understanding and exploring reaction intermediates in the deoxygenation of biooils can improve the selectivity of certain products by using zeolites of certain micropore sizes.

(2) Systematic studies should be carried out to understand the cross-interaction of biooil components and their impact on zeolite deactivation. The biooil components responsible for the higher catalyst deactivation should be identified and removed/deoxygenated earlier to prevent excessive catalyst deactivation.

(3) The use of hierarchical zeolites impregnated with nonprecious metal cations should be explored to improve the accessibility of active sites inside the zeolite framework and reduce the mass transport limitations associated with microporous zeolites. The porosity-acidity interaction in hierarchical zeolites should be investigated in detail for the efficient design of hierarchical zeolites and their use in the catalytic deoxygenation of pyrolysis oils.

(4) Complex oxygenates and phenolics can be more detrimental to catalyst activity than other biooil components. Cascade processes (comprising of a number of different heterogeneous catalysts operating at different reaction conditions), where the components of biooil can be upgraded stepwise with minimum catalyst deactivation, should be envisaged. In such a setup, the thermally unstable compounds can be removed at low temperatures (300 - 350 °C) along with partial deoxygenation over nonprecious metal-zeolite catalysts (such as Ni, Mo, Co, W, Sn, Mg, Cu, etc.). The remaining biooil fraction can then be deoxygenated at a higher temperature (~ 400 °C) in the presence of zeolite catalysts impregnated with precious/nonprecious metals.

Chapter 3

3 Materials and Methods

3.1 Sample Preparation

Drying is the most initial step to prepare an effective sample because it can greatly disturb the parameters like calorific value. The biomass of rice husk was desiccated with air for 5 days to remove the inbound moisture. After primary desiccation, at the heating temperature of 105 °C the biomass's inbound moisture was removed in an electric oven for 24 hours. Then it was ground into mortar along with a pestle and the particles were sieved through a 0.20 mm mesh screen. After sieving, a fine powder of rice husk was used because size is an important factor that influences pyrolysis [12].

Rice husk powder was loaded with zeolite catalysts (MTES-beta, beta, and commercial beta-zeolites) in the biomass to catalyst ratio of 1:0.03. Four samples were prepared, each sample weighed 3 grams and was named as follows:

- RH (Rice husk – 100%)
- RH-1 (Rice husk – MTES beta-zeolite)
- RH-2 (Rice husk – Beta-zeolite)
- RH-3 (Rice husk – Commercial beta-zeolite)

The RH consisted of 100 % rice husk as a base sample to investigate the results. The samples mentioned above were made by loading catalysts onto rice husk at 3 % mass for each. Defects-rich solid acid zeolites: The MTES beta-zeolite, beta-zeolite, and commercial beta-zeolite were incorporated in this work.

3.2 Preparation and Characterizations of Catalysts

These zeolite catalysts were prepared and provided by a Japanese partner (Division of Chemical Engineering, Graduate School of Engineering Science, Osaka University Japan). MTES beta-zeolite was prepared from the precursors using the dry gel conversion method (DGC) for each as described in [11] sing 35 % tetraethylammonium hydroxide (TEAOH) as the organic structure directing agent and methyltriethoxysilane (MTES) was utilized as a silicon source and aluminum sulfate hexadecahydrate, $Al_2(SO_4)_3 \cdot 16H_2O$

(Aldrich) as an aluminum source. Beta and commercial beta-zeolite were prepared with the same technique using a DGC method, but MTES was not used in their preparation.

3.3 Brunauer-Emmett-Teller (BET) analysis

Brunauer-Emmett-Teller (BET) analysis was performed to determine the texture properties of the catalysts. For BET analysis N_2 adsorption-desorption measurements were taken out at temperature 77 K through BELSORP-Max (MicrotracBel) to determine the surface area of all catalysts.

S_{ext} and S_{BET} are the external surface area of micropores and the specific surface area of nonporous material. S_{micro} (surface area of micropores) was calculated by the difference of S_{ext} and S_{BET}. MTES beta and beta zeolites depicted large S_{ext} as compared to the commercial beta-zeolite.

Commercial beta-zeolite has a low external surface area, which may be due to the low nucleation density of clustered crystals shown in the TEM image. Commercial beta-zeolite has the highest micropore surface area, which indicates that it is highly exposed to foreign molecules.

Table 1 Catalyst samples with their properties Si to Al ratio, S_{BET} : BET surface area, S_{ext} : external surface area and S_{micro} : micropores surface area

Catalyst	**Si/Al**	**S_{BET} (m^2g^{-1})**	**S_{ext} (m^2g^{-1})**	**S_{micro} (m^2g^{-1})**
MTES beta-zeolite	11.3	753.49	127.72	625.77
Beta-zeolite	12	691.12	284.66	406.46
Commercial beta-zeolite	12.2	849.67	18.816	830.854

3.4 X-Ray diffraction (XRD) analysis

The crystalline structure of all zeolite catalysts was observed and evaluated by the X-ray diffraction (XRD) technique. In **Figure 4**, the details of XRD were recorded on the PANalytical X'Pert-MPD diffractometer by applying Cu-Kα radiation. All three samples showed sharp peaks near 23°, that could be illustrated the unique framework zeolite's

structure. The XRD patterns of all three samples exhibit a broader peak around 7°, indicating the presence of a well-defined crystalline structure. In general, beta-zeolite is proved for highly defected intergrowth of the A, B, and C three polymorphs. Plenty of such peaks near 7° portrayed through these three polymorphs, are overlapped, ending in a wide peak at the defined value. Therefore, three beta-zeolite polymorphs can be seen by overlapping this broad peak at 7° in our samples. In all samples XRD patterns indicate that except beta-zeolite no broad and specific peaks appeared: that's why MTES addition did not significantly affect their crystalline as well as amorphous structure. The MTE beta-zeolite and beta-zeolites have attributed a bit more similarity in weak peaks compared to those of the commercial beta zeolite.

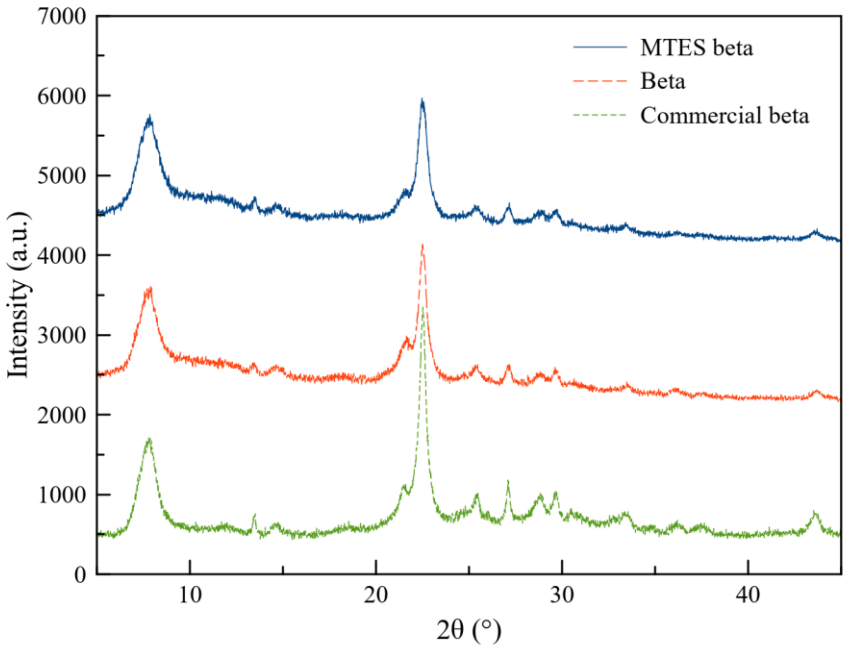

Figure 4 XRD patterns of MTES beta, beta, and commercial beta zeolites

3.5 TEM Analysis

TEM describes about the in-depth and detailed morphology of the compounds using transmitted electrons passing through them at a higher magnification range. To better

understand the morphological characteristics of the catalysts, TEM was performed for each zeolite. Clear crystal lattice fringes of MTES beta, beta, and commercial beta zeolites can be seen in **Figure 5**. The MTES beta and beta zeolite were found to be more likely in crystalline structure compared to the commercial beta-zeolite. The MTES beta-zeolite and beta-zeolite exhibits similar aggregated and compact polycrystalline nanoparticles, while the commercial beta-zeolite exhibit crystal clusters [45].

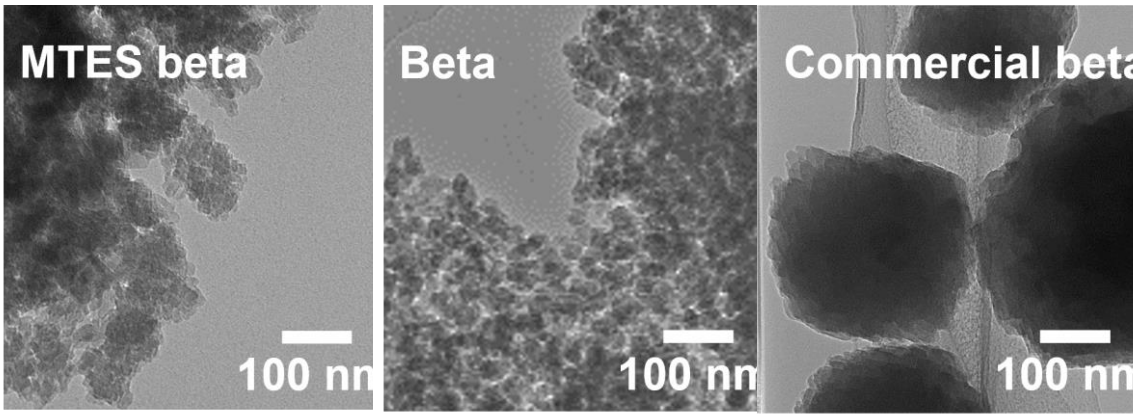

Figure 5 TEM images of a) MTES beta, b) beta and c) commercial beta zeolites: The MTES-Beta and Beta zeolites have similar crystalline structure, while the Commercial-Beta zeolite has clustered crystals

3.6 Temperature programmed desorption (TPD)

The acidic properties of the catalysts were estimated by measuring ammonia temperature programmed desorption (NH_3-TPD). TPD was performed using a BEL CAT II and a BEL mass analyzer (MicrotracBEL) that can be seen in **Figure 6**. In an inert atmosphere all samples were allowed to adsorb NH_3 at a rate of 20 ml/min for a specific time. After adsorption then the samples were allowed to heat up to 700 °C at constant heating rate for the complete desorption of ammonia. The data obtained from analyzer using online thermal conductivity detector was convoluted into the individual respective maximum desorption peaks by employing Gaussian convolution method. Through these convoluted peaks we could assess the acid sites strength which are present in the catalyst [20]. Two main desorption peaks were detected from the data analysis at low and high desorption temperatures. In **Figure 6** for all three catalysts, the first peak lies in values 215-230 °C

and the second peak lies in 340-375 °C temperature ranges. The peaks of the TPD curve in the first and second temperature ranges indicates the presence of both weak acid and strong acid sites, accordingly [21]. For commercial beta-zeolite, the first peak is sharper, and the second peak is broader in terms of ammonia desorption compared to MTES beta-zeolite and beta-zeolite, which shows that it has more promising acid strengths[45-47].

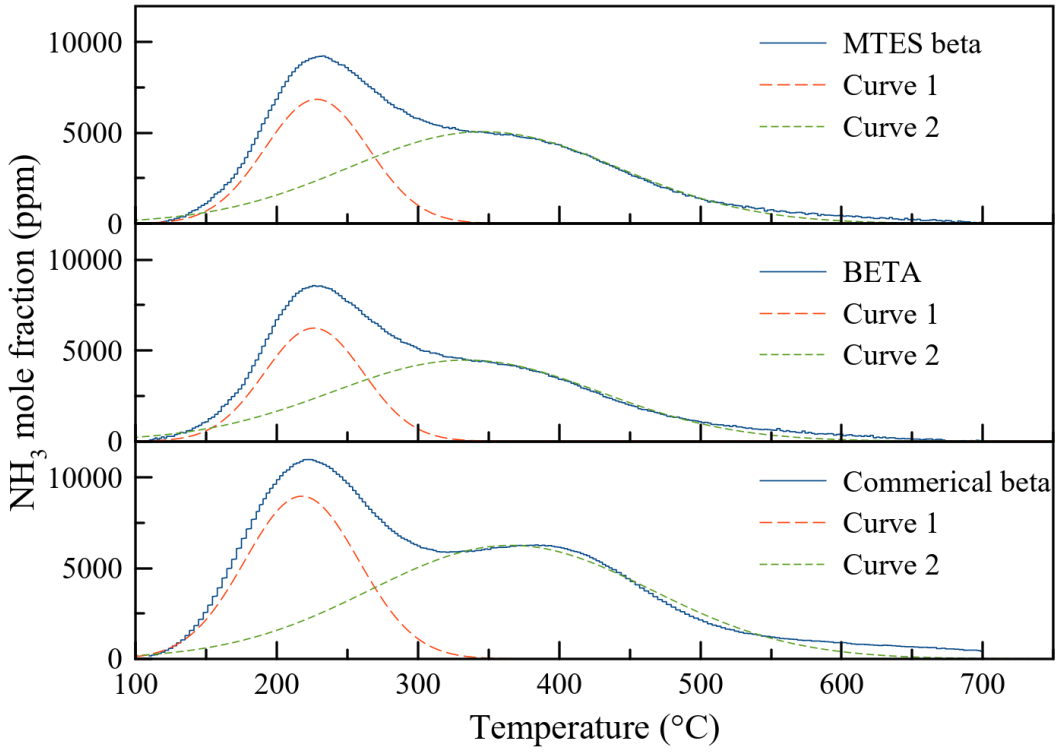

Figure 6 TPD of a) MTES beta, b) beta and c) commercial beta zeolites describe the acid sites of the catalysts by showing peaks of ammonia desorption against temperature.

3.7 Fourier Transform Infrared Spectroscopy (FTIR)

Fourier Transform Infrared (FTIR) contemplated an effective characterization technique for the identification of functional group presence in any substance. FTIR was performed on all samples by adapting a probe molecule, pyridine. Specifically, FTIR employing pyridine as a probe molecule is proven an effective tool to assess the acidity of solids[12, 48]. Band assignment was previously reported [48] as observed in the adsorbed pyridine

spectrum. The 1545 cm^{-1} band is assigned to the ν_{19b} vibration mode of pyridinium ions adsorbed at the Bronsted acid sites, and the 1455 cm^{-1} band is subjected to the ν_{19b} mode of coordinated pyridine at the Lewis acid sites [23]. The MTES beta-zeolite exhibited a bond stronger near 1455 cm^{-1} imputed to Lewis acidity as compared to beta which can be seen in **Figure 6**; though MTES promoted the Lewis acid sites formation. The bridging OH groups in the Si (OH)-Al unit portrayed the structure of the Bronsted acid; and properly illustrated Lewis acid site in zeolites.

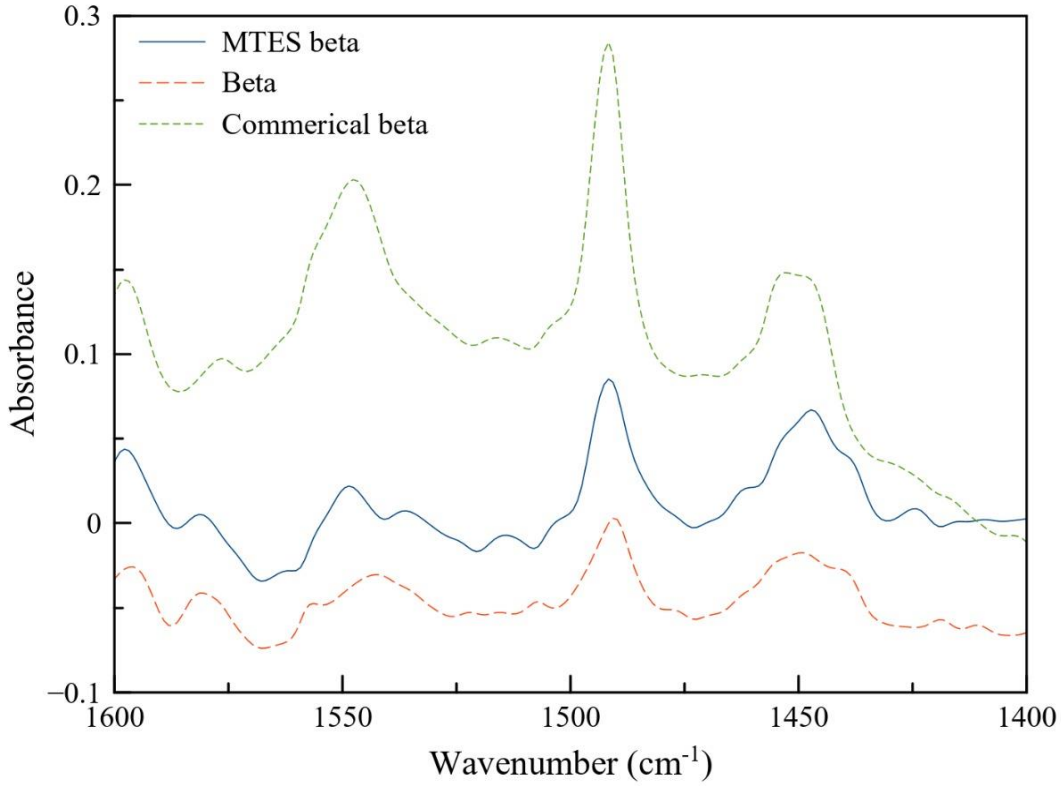

Figure 7 FTIR spectra of all three samples

3.8 Thermal Degradation Behavior of RH samples through TGA

3.8.1 Thermogravimetric Analysis

By use of TGA, the thermal degradation behavior of the rice husk was determined with different blends of the catalyst ratio. Thermogravimetric (TG) analysis was performed

under nitrogen atmosphere with a temperature range of 25 °C to 900 °C with each sample taken. For better heat transfer restrictions, the slow heating was employed to minimize the deactivation of catalyst through cracking, and coke formation and to achieve a high yield of bio-oils. The experiment was carried out three times to achieve maximum accuracy and minimize errors.

The data obtained from the TGA surely help to understand the thermal decomposition behavior during the pyrolysis process, and it can also estimate the kinetic study and the thermodynamic parameters of the different rice husk samples under pyrolysis.

3.8.2 Kinetic Study

The kinetic analysis of rice husk pyrolysis was determined by the Arrhenius law, and information about the reaction rate can be provided by this law. The general equation used for the kinetic analysis of rice husk pyrolysis was given in

$$\frac{d\alpha}{dt} = k(t)\, f(\alpha) \quad (1)$$

where

$$\alpha = \frac{m - m_i}{m_0 - m_f} \quad (2)$$

In the above equation, m_0 is the initial mass, m_i is the mass at a given time, and m_f is the final mass in grams.

$$k(T) = A \exp\left(-\frac{E}{RT}\right) \quad (3)$$

Where,

T = temperature [K]

A = Pre-exponential factor [min $^{-1}$]

R = Gas constant [0.0083 kJ/mol K]

E = Activation energy [kJ/mol]

In which n is the reaction order. For the heating rates constant β=$\frac{dt}{dT}$ Therefore, equations (2) and (3) when combined in written in the way as follows.

$$\frac{d\alpha}{dT} = \frac{A}{\beta}\exp\left(-\frac{E}{RT}\right) f(\alpha) \quad (4)$$

By the implementation of integration, a new equation is formed as

$$g(\alpha) = \int_0^{\alpha} \frac{d\alpha}{f(\alpha)} = \frac{A}{\beta}\exp\left(-\frac{E}{RT}\right) dT \quad (5)$$

In this equation, $g(\alpha)$ is the reaction model integral form. On the right side of the equation, the solution is literally impossible, so different approximation models are used to solve this complicated part of the equation.

Model Fitting Approach

3.8.3 Coats-Redfern Method (Model-Fitting Technique)

The kinetic parameters of catalytic and non-catalytic RH samples were calculated through TGA data using the Coats-Redfern method. **Table 2** lists frequently used models based on reaction modes, such as power law, phase interfacial reaction, nucleation and growth, diffusion, and chemical reaction models, were used for calculations of kinetic parameters such as the pre-exponential factor (A) and the activation energy (E) [16, 49]. The TG and derivative thermogravimetric (DTG) graphs depict the weight loss of non-catalytic and catalytic RHs with time against temperature. The Coats-Redfern method is widely used to depict the A and E to estimate the order of reaction. The general expression used for Coats-Redfern is given by

$$\ln\left[\frac{g(\alpha)}{T^2}\right] = \ln\left[\frac{AR}{\beta E}\left(1-\frac{2RT}{E}\right)\right] - \frac{E}{RT} \quad (6)$$

For the first-order reaction, g(α) would be

$$g(\alpha) = -\ln(1-\alpha)$$

so, Eq. (6) becomes

$$\ln\left[\frac{-\ln(1-\alpha)}{T^2}\right] = \ln\left[\frac{AR}{\beta E}\left(1-\frac{2RT}{E}\right)\right] - \frac{E}{RT} \quad (7)$$

Table 2 Frequently used reaction mechanisms, models, and their corresponding g(α).

Symbol	Function f(α)	g(α)
Chemical processes and mechanism non-invoking equations		
F1	First order (n=1)	-ln (1- α)
F1.5	One and a half order (n= 3/2)	$2[(1-\alpha)^{-1/2}-1]$
F2	Second-order reaction	$(1-\alpha)^{-1}-1$
Deceleratory reaction mechanism		
D1	Parabolic law	α^2
D2	Valansi equation	(1- α) ln (1- α) + α
D3	Jander equation	$[1-(1-\alpha)^{1/3}]^2$
D4	Ginstling equation	$1-(0.67\ \alpha)-(1-\alpha)^{0.67}$
Phase boundary		
Pl	Contracting cylinder	$1-(1-\alpha)^{1/2}$
Pi	Contracting sphere	$1-(1-\alpha)^{1/3}$
Sigmoidal and the random nucleation and their subsequent growth reaction mechanism		
N1.5	Avrami-Erofeev equation (n= 3/2)	$-\ln(1-\alpha)^{2/3}$
N2	Avrami-Erofeev equation (n= 2)	$-\ln(1-\alpha)^{1/2}$
N3	Avrami-Erofeev equation (n= 3)	$-\ln(1-\alpha)^{1/3}$
Acceleratory reaction mechanism		

PL	Power law (Contacting disk)	α
PL 0.5	Mampel power law (n=1/2)	$\alpha^{1/2}$

Using the reaction at 10 °C/min, the curve of g(α) versus 1/T was obtained under the different catalytic pyrolysis. The slope and intercepts of the curves ln g(α) versus 1/T were used to calculate the energy of activation when each curve was divided into two sections, based on its linearity. The precision of this model-free kinetic is indicated by the value of the correlation coefficient (R^2).

3.8.4 Model Free Approach

3.8.4.1 Flynn-Wall-Ozawa Method

This model is used to calculate E based on degree of conversion. Calculated values fluctuates with conversion as the reaction progress. This model is frequently used for estimation of merged dense proellent and is appropriate for inquiry of diverse resources. General expression of Flynn-Wall-Ozawa method can be seen below:

$ln\beta = \ln(AERg(\alpha)) - 5.523 - 1.0518(ERT)$

3.8.4.2 Friedman Method

It is renowned model among investigators in the arena of energetic ingredients. It is type of model free approch. General expression of Friedman model can be seen below:

$\ln(\beta d(\alpha)dT) = \ln[Af(\alpha)] - ERT$

Kinetic constraints canbe premeditated by drawing a graph between $\ln(\beta_{d\alpha dt})$ versus 1/T against different degrees of conversion and different heating rates.

3.8.4.3 Popescu Method

However, as E_a varies with α Flynn-Wall-Ozawa Method creates systematic errors, which can be minimized or foresighted by using integral segments of $\Delta\alpha$ as in the case of Popescu method.

$\ln(\beta T_{\alpha - T_{\alpha - \Delta\alpha}}) = const - 2E_aR(T_\alpha + T_{\alpha - \Delta\alpha})$

where $\Delta\alpha$ is the conversion interval, $T_{\alpha-\Delta\alpha}$ is the absolute temperature at $\alpha-\Delta\alpha$ and T_{α} is the corresponding temperature to α.

3.8.5 Thermodynamic Analysis

3.8.5.1 Thermodynamic Parameters

Various thermodynamic parameters, including the enthalpy change, the Gibbs free energy change, and the entropy change, can be obtained from thermogravimetric (TG) analysis. On the basis of the kinetic data, the parameters of thermodynamics can be obtained from the given equations under:

$$\Delta H = E - RT \quad \textbf{(8)}$$

$$\Delta G = E + RT_m \ln\left(\frac{K_B T}{hA}\right) \quad \textbf{(9)}$$

$$\Delta S = \frac{\Delta H - \Delta G}{T_m} \quad \textbf{(10)}$$

where K_b is the Boltzmann constant, and the value is $1.381 \times 10^{-23} m^2 kg/s^{-2} K^{-1}$ while, the T_m is the peak temperature or maximum temperature at which the decomposition will occur. h is the Planck constant, and the value of the Planck constant is 6.626×10^{-34} m^2.kg/s. R is the universal gas constant equal to 0.008314 kJ/mol K.

Chapter 4

4 Result and Discussion

4.1 Thermal degradation Behavior of catalytic and non-catalytic rice husk through TGA

The kinetic parameters of catalytic and non-catalytic RH samples were calculated through the TGA data using model fitting Coats-Redfern method. Frequently used models based on different reaction mechanisms such as power law, phase interfacial reaction, nucleation and growth, diffusion and chemical reaction models were used for calculations of kinetic parameters such as the pre-exponential factor (A) and activation energy (E) [16, 49] **Figure 8** shows the thermogravimetric TG and DTG graphs that depict the weight loss of non-catalytic and catalytic RH with time versus temperature.

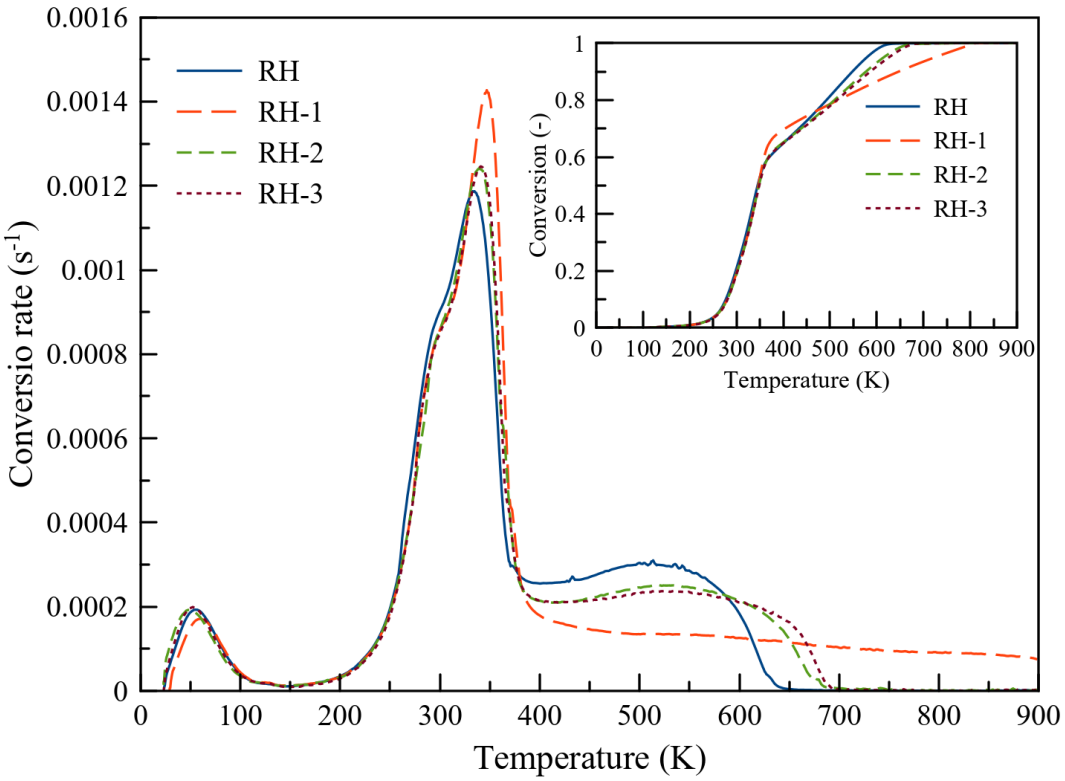

Figure 8 TG and DTG Curves of RH, RH-1, RH-2, and RH-3 samples

In the DTG plot curves, the peaks indicate that the maximum mass loss occurred at three peak temperatures. Thus, thermal degradation is divided into three phases. The first phase (0-100 °C) is found below the temperature of 100 °C, which shows that the moisture loss is 5 % of the total mass loss. The bound moisture is vaporized in the first phase. In the second phase (200-400 °C), maximum mass loss was observed, as primary decomposition reactions took place in this phase for both non-catalytic and catalytic RH pyrolysis. The heat propagated in the particles, and a large part of hemicellulose and cellulose was degraded in this temperature range. The C-C, C-OH, C=C bonds were broken to a greater extent, which is why the maximum mass loss was carried out in the temperature range of 250-360 °C for both non-catalytic and catalytic RH samples [15, 16]. The third peak in mass loss was observed in a temperature range of 400-700 °C [12, 16]. The decomposition of lignin requires a wider range (150-900 °C) due to its complex polymeric heat-resistant structures [12, 50]. Lignin molecules have a three-dimensional cross-linked array due to the presence of hydroxyl and carboxyl groups [49, 51]. From **Figure 8**, the maximum mass loss of the third phase was observed between the temperature range of 450-550 °C.

4.2 Kinetic and Thermodynamic Analysis through Model Fitting Approach

4.2.1 Kinetic Parameters through Coats and Redfern Method

The Coats-Redfern method is one of the most widely used tools for assessing thermokinetics by using TGA data at a single heating rate. As a non-isothermal and fitting model, it estimates the kinetic triplets (activation energy (E), pre-exponential factor (A), and reaction model $f(\alpha)$). These thermokinetic studies led to the best estimate of the thermodynamic parameters. Five types of reaction mechanism models (reaction order model, diffusion model, phase boundary model, Avrami-Erofeev equation model, and power law) developed by the Coats-Redfern method were applied in non-catalytic and catalytic RH to calculate and analyze the kinetic behavior. According to the maximum mass loss from TG data, the curves were categorized into two sections: Section I (250-360 °C) and Section II (450-550 °C) according to the linearity characteristics. The slope

of $\ln[g(\alpha)/T^2]$ versus 1/T corresponded to -E/R for the calculation of the activation energy of each sample as shown in Table 3, while the pre-exponential factor, A, can be obtained from the intercept of the straight line [52].

Table 3 Kinetic parameters, activation energy, linear regression, and pre-exponential factor of all solid-state reaction mechanisms

Models		Samples	Section-I (250-360 °C)			Section-II (450-550 °C)		
			E (kJ/mol)	R^2	A (s^{-1})	E (kJ/mol)	R^2	A (s^{-1})
Order Reaction Model	F1	RH	52.6	0.99	3.73E+03	21.9	0.95	2.77
		RH-1	54.4	0.99	4.55E+03	1.8	0.98	0
		RH-2	51.3	0.99	2.52E+03	10.3	0.96	0.18
		RH-3	51.9	0.99	2.84E+03	8.6	0.96	0.11
	F1.5	RH	58.5	0.99	1.60E+04	43.7	0.94	296.53
		RH-1	60.1	0.99	1.82E+04	2.7	0.95	0.02
		RH-2	56.8	0.99	9.44E+03	22	0.96	3.76
		RH-3	57.1	0.99	1.02E+04	18.9	0.97	1.93
	F2	RH	13.2	0.8	1.16E+00	61.2	0.92	14409.6

		RH-1	12.4	0.75	8.50E-01	3.2	0.92	0.05
		RH-2	11	0.77	5.78E-01	27.7	0.95	24.27
		RH-3	10.5	0.72	5.03E-01	23.5	0.95	10.02
Diffusion model	D1	RH	93.9	0.99	6.28E+02	7.5	0.99	0.04
		RH-1	98.1	1	1.43E+07	3.1	1	0
		RH-2	93.1	0.99	5.92E+06	4.3	0.99	0.01
		RH-3	94.6	1	8.06E+06	3.6	1	0.01
		RH-C	93.6	0.99	3.11E+03	9.2	1	0.06
	D2	RH	100.3	0.99	1.86E+07	17.2	0.99	0.3
		RH-1	104.4	1	3.15E+07	0.1	0.72	0
		RH-2	99	1	1.21E+07	10.8	0.99	0.06
		RH-3	100	1	1.60E+06	9.6	0.99	0.04
	D3	RH	107.3	0.99	2.29E+07	34.5	0.98	3.81
		RH-1	111.2	1	3.61E+07	4.2	0.99	0

		RH-2	105	1	1.26E+07	21.1	0.98	0.23
		RH-3	106.7	1	1.64E+07	18.8	0.99	0.14
	D4	RH	102.7	0.99	7.22E+06	22.7	0.98	0.26
		RH-1	106.6	0.99	1.19E+07	1.3	0.98	0
		RH-2	101.2	0.99	4.44E+06	14.2	0.99	0.04
		RH-3	102.6	1	5.85E+06	12.6	0.99	0.02
Phase Boundary Model	Pl	RH	48.5	0.99	4.36E+02	12.3	0.96	0.08
		RH-1	49.1	1	6.22E+02	-5.4	1	0
		RH-2	46.4	1	3.69E+02	1.7	0.83	0
		RH-3	47.1	1	4.26E+02	0.8	0.62	0
	Pi	RH	49	1	4.98E+02	11.1	0.96	0.06
		RH-1	50.9	1	6.32E+02	-4.3	0.99	0
		RH-2	48	1	3.67E+02	4.3	0.93	0.01
		RH-3	48.7	1	4.20E+02	3.2	0.92	0

Avrami-Erofeev	N1.5	RH	32.1	1	4.52E+01	10.4	0.91	0.17
		RH-1	33.3	1	5.19E+01	-5.5	1	-0.01
		RH-2	32.5	1	4.70E+01	-5.5	0.99	-0.01
		RH-3	31.6	1	3.74E+01	1.5	0.67	0.01
	N2	RH	21.6	1	4.02E+00	4.5	0.79	0.03
		RH-1	22.4	1	4.49E+00	-7.4	1	-0.01
		RH-2	21.8	1	4.16E+00	-7.4	1	-0.01
		RH-3	21.2	0.99	3.48E+00	-2.1	0.9	0
	N3	RH	11	0.99	2.71E-01	-1.4	0.46	0
		RH-1	11.5	1	2.96E-01	-9.3	1	-0.01
		RH-2	11.1	1	2.80E-01	-9.2	1	-0.01
		RH-3	10.7	0.99	2.44E-01	-5.8	1	-0.01
Power Law	PL 1	RH	42.1	0.99	2.72E+02	-2.7	0.99	0
		RH-1	44.2	1	3.71E+02	-8	1	0

		RH-2	41.8	1	2.34E+02	-4.2	1	0
		RH-3	42.6	1	2.76E+02	-4.6	1	0
	PL 0.5	RH	16.3	0.99	9.17E-01	-7.7	1	0
		RH-1	17.3	0.99	1.10E+00	-10.5	1	0
		RH-2	16.1	0.99	8.45E-01	-8.5	1	0
		RH-3	16.5	0.99	9.32E-01	-8.7	1	0

Order Reaction Model

In Section I, the correlation factor R^2 values for F1 and F2 remained 0.99 for both non-catalytic and catalytic RH samples, but for F2 it varies from 0.75 to 0.79 in catalytic RH samples and 0.8 for the non-catalytic RH sample. In Section II, the R^2 values range from 0.92 to 0.98 for both non-catalytic and catalytic RH samples. In Section I for F1 and F1.5, the activation energy of RH-1 is greater than that of the RH sample, and for all orders of catalytic RH samples, E is less than RH. In section II for F1, F1.5 and F2 all catalytic RH samples have a drastic reduction in activation energy values as compared to section I which depicts zeolite catalysts aided lignin decomposition. In Sections I and II, the values of pre-exponential factor A of all catalytic RH samples were less than RH except for F1, F1.5 RH-1 in Section I correspond to high activation energy values.

Diffusion Model

In Section I, the linear regression with the R^2 values for D1, D2, D3, and D4 remained approximately the same 0.99 for all samples. In Section II, linear regression with R^2 values for D1, D2, D3 and D4 remained approximately 0.99 for all samples except for D2 RH-1 which was 0.72. In Section I, the activation energies for D1, D2, D3, and D4 of all catalytic RH samples have a minute difference from the RH sample. In Section II, greater differences were found in the activation energies for D1, D2, D3 and D4 of all catalytic RH samples. In Section I, the value of the pre-exponential factor A for RH-2 D1 is greater than RH, since the corresponding E has a lower value. The D2, D3, and D4 models described better results.

Phase-Boundary Model

In Section I, the correlation factor R^2 values for Pl and Pi remained 0.99 for both non-catalytic and catalytic RH samples. In Section II R^2 values for Pi varied from 0.92 to 0.99 but for P1 - RH-2 and RH-3 it was 0.83 and 0.62. In Section I for the Pl and Pi activation energies of all catalytic RH samples, there is a minute difference from the RH sample, although the RH-1 E value is greater than RH. In Section II, the activation energies of Pl and Pi of all catalytic RH samples were found to be lower than those of the RH sample, and the RH-1 E values are negative, implying a complex reaction mechanism that may have different elementary reactions at different rates [53]. In Section II for both Pl and Pi, the values of the pre-exponential factor A for RH-1 are negative corresponding to negative E. Pl and Pi described the results with less ambiguity for all samples except RH-1.

Avrami-Erofeev Model

In Section I the correlation factor R^2 values for N1.5, N2 and N3 were approximately 0.99 but for Section II it is 0.67 for RH-3 N1.5. In Section I for the activation energies of mechanisms; N1.5, N2, and N3, for all catalytic RH samples had fewer differences, but in Section II the values were mostly negative. A similar trend was followed for pre-exponential factor values.

Power-Law Model

In Sections I and II, the correlation factor R^2 values for PL1 and PL0.5 were found to be approximately 0.99 in the case of all catalytic and non-catalytic RH samples. In Section I, the activation energies of PL1 and PL0.5 of all catalytic RH samples had little differences compared to the RH sample, but in Section II, all values are negative for all samples and the same trend was followed for the pre-exponential factor.

According to the analysis of the kinetic parameters (E_a, A, and R^2), analysis of all reaction models F1, F1.5, D2, D3, and D4 described appropriate results that are approximation and synergistic to each other for both sections. It can be summarized from the calculations and results that non-catalytic RH pyrolysis in Section I follows a first-order reaction in general. However, all diffusion-controlled, phase boundary, and Avrami Erofeev models seemed more promising in depicting non-catalytic and catalytic RH pyrolysis (as high values of the correlation-coefficient were observed). In section II diffusion (one-dimensional), and acceleratory reaction mechanism models (Power law and Mample Power Law) expressed the highest correlation coefficient values. Therefore, in terms of the Coats-Redfern method, the three-dimensional D3 diffusion-controlled model exhibits (R^2=0.999) the best linearity for Section I and the power law PL showed (R2 = 1.00) the best linearity for Section II. Parallel to the diffusion-controlled model other models also described high values for the correlation coefficient, but they might be suitable for defining the complex pyrolysis of both catalytic and non-catalytic RH. Activation energy of all catalyzed samples was significantly reduced for the samples of RH-2 and RH-3 compared to non-catalytic RH except RH-1 in section-I. In Section II, a notable decrease in the activation energies of the RH-1, RH-2, and RH-3 samples was found as compared to the RH sample. Thus, it can be understood that MTES beta-zeolite has no significant effect on pyrolysis in section I and commercial zeolite has no promising results in section II. Beta-zeolite and commercial beta-zeolite gave better results for all reaction models in both sections by lowering the activation energies.

4.3 Thermodynamic Analysis of RH Catalytic Pyrolysis

Thermodynamic parameters are the change ΔH, ΔG and ΔS, as illustrated in Table 6, which were analyzed by estimating the temperatures corresponding to the maximum conversions from TGA data. This peak temperature denotes the maximum mass loss achieved at this value [54-56]. Enthalpy is the total heat content of a system, and the change in enthalpy represents the heat released or absorbed at constant pressure [57]. The ΔG tells about the intensity of output that can be achieved through the system. It also defines the increase in the formation of activated complexes [58, 59]. ΔS is an index that indicates the disorder of a system. In section-I ΔH was remained positive for all solid-state reaction models, showing that an external source is needed to provide sufficient energy to molecules for the completion of the reaction; in other words, it exhibits the endothermic behavior of reactions [60]. Higher values of ΔH shows that it will take longer for conversion or it has a potential energy barrier for the formation of products [9].In Section II of the order-based reaction, diffusion, and phase boundary models, the non-catalytic RH sample's ΔH values were found to be positive while the latter two are negative; and for catalytic samples, RH-1 and RH-2 have negative ΔH while the latter two exhibit all negative values. Negative ΔH shows that the reactions in section II are mostly exothermic in nature. In both sections, it can be seen in that ΔH value increases corresponding to the increase in activation energy. ΔG provides information on the addition of reactants to the total energy of the system or the formation of an activated complex. In Section I, ΔG values show for all reaction models in catalytic and non-catalytic RH samples that reactants were consumed, and an activated complex was formed, while in Section II for the Avrami and Power law reaction models ΔG could not be predicted. In the table for the first three reaction models in section-I ΔG values of G were significantly higher than in section I, indicating disorder and changes in the heat flow [26]. In all reaction models for non-catalytic and catalytic RH samples in both section ΔS remained negative. This trend describes that the disorder that occurred in the bond breakage of the product was low compared to the primary reactants [61]. Degree of

arrangement of carbon deposits in RH samples can also be assessed by this change, and indicating a mild pattern of activated complex formation [62].

Table 4 Thermodynamic Parameters; (ΔH) Change in Enthalpy, (ΔG) Gibbs free energy and (ΔS) Change in Entropy of all Solid-state reaction mechanisms

Models		Samples	Section I (250-360 °C)			Section II (450-550 °C)		
			ΔH	ΔG	ΔS	ΔH	ΔG	ΔS
Order Reaction Model	F1	RH	47.4	188.8	-0.225	15.4	241	-0.287
		RH-1	49.1	192.2	-0.224	-4.9	271.9	-0.342
		RH-2	46	191.3	-0.229	3.8	248.9	-0.31
		RH-3	46.6	191.8	-0.228	1.9	255.2	-0.314
	F1.5	RH	53.3	187.1	-0.213	37.2	232.3	-0.248
		RH-1	54.8	190.5	-0.212	-4.1	262.8	-0.329
		RH-2	51.5	189.9	-0.218	15.4	240.5	-0.284
		RH-3	51.8	190.2	-0.217	12.2	246.4	-0.29
	F2	RH	8	191.6	-0.292	54.7	224.4	-0.216
		RH-1	7.1	195.9	-0.295	-3.5	256.8	-0.321

		RH-2	5.7	195.4	-0.298	21.1	234	-0.269
		RH-3	5.2	196.2	-0.299	16.7	239.9	-0.276
Diffusion model	D1	RH	88.6	190	-0.161	1	255	-0.323
		RH-1	92.7	193	-0.157	-3.6	276.9	-0.346
		RH-2	87.8	192.1	-0.164	-2.3	261	-0.333
		RH-3	89.3	192.3	-0.161	-3.2	267.7	-0.335
	D2	RH	95.1	192	-0.154	10.7	250.8	-0.305
		RH-1	99	195.1	-0.15	-6.6	294.4	-0.372
		RH-2	93.7	194.2	-0.158	4.2	256.6	-0.319
		RH-3	4.7	116.3	-0.175	2.8	262.6	-0.322
	D3	RH	102.1	198	-0.153	28	251.6	-0.284
		RH-1	105.9	201.2	-0.149	-2.6	277.5	-0.346
		RH-2	99.7	200	-0.158	14.5	258.2	-0.308
		RH-3	101.4	200.6	-0.156	12.1	264.1	-0.312

	D4	RH	97.4	199.3	-0.162	16.2	257.5	-0.307
		RH-1	101.3	202.5	-0.158	-5.5	287.8	-0.362
		RH-2	95.9	201.7	-0.166	7.6	263.5	-0.323
		RH-3	97.3	201.9	-0.164	5.8	269.7	-0.327
Phase-Boundary Model	Pl	RH	43.3	195.9	-0.243	5.8	254.5	-0.316
		RH-1	43.8	197.5	-0.24	-12.1	-	-
		RH-2	41.1	196.6	-0.244	-4.9	268.3	-0.345
		RH-3	41.8	197	-0.243	-5.9	278.9	-0.353
	Pi	RH	43.8	195.7	-0.242	4.6	255.1	-0.318
		RH-1	45.6	199.2	-0.24	-11	-	-
		RH-2	42.7	198.3	-0.245	-2.3	263.9	-0.336
		RH-3	43.4	198.7	-0.243	-3.6	271.4	-0.341
Avrami-Erofeev	N1.5	RH	26.9	191.3	-0.262	3.9	247.7	-0.31
		RH-1	28	194.9	-0.261	-6.2	-	-

		RH-2	27.2	193.6	-0.262	-12.1	-	-
		RH-3	26.3	194.5	-0.264	-5.2	268.3	-0.339
	N2	RH	16.3	193.4	-0.282	-2	254.1	-0.326
		RH-1	17.1	197	-0.281	-14.1	-	-
		RH-2	16.5	195.7	-0.282	-14	-	-
		RH-3	15.9	196.6	-0.283	-8.8	-	-
	N3	RH	5.7	196.9	-0.304	-7.9	-	-
		RH-1	6.2	200.6	-0.304	-16	-	-
		RH-2	5.9	199.3	-0.304	-15.8	-	-
		RH-3	5.4	200.3	-0.305	-12.5	-	-
Power Law	PL 1	RH	36.9	192	-0.247	-9.2	-	-
		RH-1	38.9	195.4	-0.244	-14.8	-	-
		RH-2	36.5	194.4	-0.248	-10.8	-	-
		RH-3	37.3	194.8	-0.247	-11.3	-	-

	PL 0.5	RH	11.1	195.9	-0.294	-14.3	-	-
		RH-1	12	199.4	-0.293	-17.2	-	-
		RH-2	10.8	198.5	-0.295	-15.1	-	-
		RH-3	11.2	198.9	-0.294	-15.4	-	-

Conclusion

Coats-Redfern method was employed using different reaction mechanism models to analyze the kinetic behavior of both non-catalytic and catalytic RH. Nature of biomass pyrolysis was investigated by performing a TGA of all the prescribed samples in this study. The TGA and DTG data curves for the catalytic and non-catalytic pyrolysis of RH were analyzed by identifying two sections corresponding to the maximum mass losses: Section I (250-360 °C) & Section II (450-550 °C) respectively. According to the analysis of the kinetic triplet (E, A, and R^2) analysis of all reaction models F1, F1.5, D2, D3, and D4 described appropriate results that are in approximation with each other for both sections. Therefore, regarding the Coats-Redfern method, the three-dimensional D3 diffusion-controlled model exhibits best linearity regarding to the Section I and Power law PL showed the best linearity for Section II. From the activation energy trends, it can be understood that MTES beta-zeolite has no significant effect on pyrolysis in Section I and has promising results in Section II. The beta-zeolite and commercial beta-zeolite gave better results for all reaction models in both sections. In section-I ΔH was remained positive for all reaction models, showing that an external source is needed to provide molecules sufficient energy for reaction completion; in other words, it exhibits the endothermic behavior of reactions. In Section II, order reaction, diffusion and phase boundary models, the ΔH values of the non-catalytic RH samples were observed to be positive, while the latter two exhibited negative; and for catalytic samples, RH-1 and RH-2 have negative ΔH while the latter two exhibit all negative values. In Section I, ΔG values show for all reaction models in catalytic and non-catalytic RH samples that reactants were consumed, and an activated complex was formed, while in Section II for the Avrami and Power law reaction models ΔG could not be predicted. In the table for the first three reaction models in Section I, ΔG values were recorded significantly higher than in Section I, so it can hypothesize disorder and changes in the heat flow. In all reaction models for both non-catalytic and catalytic RH samples in both section ΔS remained negative. This trend describes the disorder that occurred in product bond breakage as low compared to the primary reactants.

Future Recommendations

Based on the above results, for more exploring in pyrolysis process, the following future work is recommended:

- In pyrolyzer units the addition of the above-mentioned beta zeolites can enhance the quality of biofuel that could be prolonged by providing new techniques and optimum process condition such as temperature, size of feedstock and residence time.
- A computational model should be established to enhance the physical, chemical and reaction parameters which will help to design the process.
- Different kinetic model should be established at multiple heating rates to investigate the best functioning condition to design the catalytic pyrolysis process to obtain the maximum yield with lower investment.
- It should be developed on commercial scale because Rice husk can be better the alternative for fossil fuels, thermal degradation can reduce environmental hazards, and usage of catalyst make the process greener as compared to the conventional pyrolysis.

References

[1] G. Bensidhom, A. B. H. Trabelsi, and S. Ceylan, "Insights into pyrolytic feedstock potential of date palm industry wastes: kinetic study and product characterization," *Fuel*, vol. 285, p. 119096, (2021).

[2] F. Sher, M. A. Pans, D. T. Afilaka, C. Sun, and H. Liu, "Experimental investigation of woody and non-woody biomass combustion in a bubbling fluidised bed combustor focusing on gaseous emissions and temperature profiles," *Energy*, vol. 141, pp. 2069-2080, (2017).

[3] Y. Shen, J. Wang, X. Ge, and M. Chen, "By-products recycling for syngas cleanup in biomass pyrolysis–An overview," *Renewable and Sustainable Energy Reviews*, vol. 59, pp. 1246-1268, (2016).

[4] S. S. Shukla, R. Chava, S. Appari, A. Bahurudeen, and B. V. R. Kuncharam, "Sustainable use of rice husk for the cleaner production of value-added products," *Journal of Environmental Chemical Engineering*, vol. 10, no. 1, p. 106899, 2022.

[5] I. Quispe, R. Navia, and R. Kahhat, "Energy potential from rice husk through direct combustion and fast pyrolysis: a review," *Waste management*, vol. 59, pp. 200-210, (2017).

[6] O. Knight, "Assessing and mapping renewable energy resources," 2016.

[7] Y. Shen, P. Zhao, Q. Shao, D. Ma, F. Takahashi, and K. Yoshikawa, "In-situ catalytic conversion of tar using rice husk char-supported nickel-iron catalysts for biomass pyrolysis/gasification," *Applied Catalysis B: Environmental*, vol. 152, pp. 140-151, (2014).

[8] H. C. Ong, W.-H. Chen, A. Farooq, Y. Y. Gan, K. T. Lee, and V. Ashokkumar, "Catalytic thermochemical conversion of biomass for biofuel production: A comprehensive review," *Renewable and Sustainable Energy Reviews*, vol. 113, p. 109266, (2019).

[9] M. S. Ahmad *et al.*, "Pyrolysis, kinetics analysis, thermodynamics parameters and reaction mechanism of Typha latifolia to evaluate its bioenergy potential," *Bioresource Technology*, vol. 245, pp. 491-501, 2017/12/01/ (2017).

[10] W. Khan, X. Jia, Z. Wu, J. Choi, and A. C. K. Yip, "Incorporating hierarchy into conventional zeolites for catalytic biomass conversions: A review," *Catalysts*, vol. 9, no. 2, p. 127, (2019).

[11] S. Kokuryo, K. Miyake, Y. Uchida, A. Mizusawa, T. Kubo, and N. Nishiyama, "Defect engineering to boost catalytic activity of Beta zeolite on low-density polyethylene cracking," *Materials Today Sustainability*, vol. 17, p. 100098, (2022).

[12] S. R. Naqvi, Y. Uemura, N. Osman, and S. Yusup, "Kinetic study of the catalytic pyrolysis of paddy husk by use of thermogravimetric data and the Coats–Redfern model," *Research on Chemical Intermediates*, vol. 41, no. 12, pp. 9743-9755, (2015).

[13] J. Prasara-A and S. H. Gheewala, "Sustainable utilization of rice husk ash from power plants: A review," *Journal of Cleaner Production*, vol. 167, pp. 1020-1028, (2017).

[14] S. R. Naqvi, Y. Uemura, and S. B. Yusup, "Catalytic pyrolysis of paddy husk in a drop type pyrolyzer for bio-oil production: The role of temperature and catalyst," *Journal of Analytical and Applied Pyrolysis*, vol. 106, pp. 57-62, (2014).

[15] S. R. Naqvi *et al.*, "Synergistic effect on co-pyrolysis of rice husk and sewage sludge by thermal behavior, kinetics, thermodynamic parameters and artificial neural network," *Waste Management*, vol. 85, pp. 131-140, (2019).

[16] A. C. M. Loy *et al.*, "Comparative study of in-situ catalytic pyrolysis of rice husk for syngas production: kinetics modelling and product gas analysis," *Journal of Cleaner Production*, vol. 197, pp. 1231-1243, (2018).

[17] Z. Qin, B. Shen, X. Gao, F. Lin, B. Wang, and C. Xu, "Mesoporous Y zeolite with homogeneous aluminum distribution obtained by sequential desilication–dealumination and its performance in the catalytic cracking of cumene and 1, 3, 5-triisopropylbenzene," *Journal of Catalysis*, vol. 278, no. 2, pp. 266-275, (2011).

[18] H. Mahmood, A. Shakeel, A. Abdullah, M. I. Khan, and M. Moniruzzaman, "A Comparative Study on Suitability of Model-Free and Model-Fitting Kinetic

Methods to Non-Isothermal Degradation of Lignocellulosic Materials," *Polymers,* vol. 13, no. 15, (2021).

[19] A. Dhaundiyal, S. B. Singh, M. M. Hanon, and R. Rawat, "Determination of Kinetic Parameters for the Thermal Decomposition of Parthenium hysterophorus," *Environmental and Climate Technologies,* vol. 22, no. 1, pp. 5-21, (2018).

[20] D. K. Ratnasari, W. Yang, and P. r. G. Jönsson, "Kinetic study of an H-ZSM-5/Al–MCM-41 catalyst mixture and its application in lignocellulose biomass pyrolysis," *Energy & Fuels,* vol. 33, no. 6, pp. 5360-5367, (2019).

[21] M. W. Nolte and B. H. Shanks, "A perspective on catalytic strategies for deoxygenation in biomass pyrolysis," *Energy technology,* vol. 5, no. 1, pp. 7-18, (2017).

[22] J. L. C. W. Pimenta, M. de Oliveira Camargo, R. B. Duarte, O. A. A. dos Santos, and L. M. de Matos Jorge, "Deoxygenation of vegetable oils for the production of renewable diesel: Improved aerogel based catalysts," *Fuel,* vol. 290, p. 119979, (2021).

[23] C. H. Ko, S. H. Park, J.-K. Jeon, D. J. Suh, K.-E. Jeong, and Y.-K. Park, "Upgrading of biofuel by the catalytic deoxygenation of biomass," *Korean Journal of Chemical Engineering,* vol. 29, no. 12, pp. 1657-1665, (2012).

[24] J. L. C. W. Pimenta, M. de Oliveira Camargo, R. B. Duarte, O. A. A. dos Santos, and L. M. de Matos Jorge, "A novel kinetic model applied to heterogeneous fatty acid deoxygenation," *Chemical Engineering Science,* vol. 230, p. 116192, (2021).

[25] A. Zheng *et al.*, "Controlling deoxygenation pathways in catalytic fast pyrolysis of biomass and its components by using metal-oxide nanocomposites," *Iscience,* vol. 23, no. 1, p. 100814, (2020).

[26] M.-Y. Choo *et al.*, "Deoxygenation of triolein to green diesel in the H2-free condition: Effect of transition metal oxide supported on zeolite Y," *Journal of Analytical and Applied Pyrolysis,* vol. 147, p. 104797, (2020).

[27] N. Muradov, "Low-carbon production of hydrogen from fossil fuels," in *Compendium of hydrogen energy*: Elsevier, (2015), pp. 489-522.

[28] Q. Zhou, S. Yang, H. Wang, Z. Liu, and L. Zhang, "Selective deoxygenation of biomass volatiles into light oxygenates catalysed by S-doped, nanosized zinc-rich scrap tyre char with in-situ formed multiple acidic sites," *Applied Catalysis B: Environmental*, vol. 282, p. 119603, (2021).

[29] M. M. Rahman, R. Liu, and J. Cai, "Catalytic fast pyrolysis of biomass over zeolites for high quality bio-oil–a review," *Fuel Processing Technology*, vol. 180, pp. 32-46, (2018).

[30] D. J. Mihalcik, C. A. Mullen, and A. A. Boateng, "Screening acidic zeolites for catalytic fast pyrolysis of biomass and its components," *Journal of Analytical and Applied Pyrolysis*, vol. 92, no. 1, pp. 224-232, (2011).

[31] P. S. Rezaei, H. Shafaghat, and W. M. A. W. Daud, "Production of green aromatics and olefins by catalytic cracking of oxygenate compounds derived from biomass pyrolysis: A review," *Applied Catalysis A: General*, vol. 469, pp. 490-511, 2014/01/17/ (2014).

[32] T. Ennaert *et al.*, "Potential and challenges of zeolite chemistry in the catalytic conversion of biomass," *Chemical Society Reviews*, 10.1039/C5CS00859J vol. 45, no. 3, pp. 584-611, (2016).

[33] H. Shi, K. K. Ramasamy, R. Ma, and H. Wang, "12 - Nanoporous catalysts for biomass conversion," in *Nanoporous Materials for Molecule Separation and Conversion*, J. Liu and F. Ding, Eds.: Elsevier, (2020), pp. 387-440.

[34] L. Kasmiarno, S. Steven, J. Rizkiana, E. Restiawaty, and Y. Bindar, "Kinetic studies and performance analysis of Indonesian rice husk pyrolysis," *IOP Conference Series: Materials Science and Engineering*, vol. 1143, p. 012067, 04/01 (2021).

[35] J. H. Park, Y. K. Park, and Y.-M. Kim, "Kinetic analysis and catalytic pyrolysis of spent medicinal herb over HZSM-5 and HY," *Environmental Research*, vol. 187, p. 109632, 2020/08/01/ (2020).

[36] Y. M. Wang and J. Wang, "Catalytic performances of HZSM-5, NaY and MCM-41 in two-stage catalytic pyrolysis of pinewood," *IOP Conference Series: Earth and Environmental Science*, vol. 40, p. 012015, 2016/08 (2016).

[37] H. Zhang *et al.*, "Study on Pyrolysis of Pine Sawdust with Solid Base and Acid Mixed Catalysts by Thermogravimetry–Fourier Transform Infrared Spectroscopy and Pyrolysis–Gas Chromatography/Mass Spectrometry," *Energy & Fuels,* vol. 28, no. 7, pp. 4294-4299, 2014/07/17 (2014).

[38] P. Sudarsanam, E. Peeters, E. V. Makshina, V. I. Parvulescu, and B. F. Sels, "Advances in porous and nanoscale catalysts for viable biomass conversion," *Chemical Society Reviews,* vol. 48, no. 8, pp. 2366-2421, (2019).

[39] C. Perego and A. Bosetti, "Biomass to fuels: The role of zeolite and mesoporous materials," *Microporous and Mesoporous Materials,* vol. 144, no. 1-3, pp. 28-39, (2011).

[40] R. Černý, M. Kubů, and D. Kubička, "The effect of oxygenates structure on their deoxygenation over USY zeolite," *Catalysis today,* vol. 204, pp. 46-53, (2013).

[41] M. W. Nolte, J. Zhang, and B. H. Shanks, "Ex situ hydrodeoxygenation in biomass pyrolysis using molybdenum oxide and low pressure hydrogen," *Green Chemistry,* vol. 18, no. 1, pp. 134-138, (2016).

[42] M. Ozagac, C. Bertino-Ghera, D. Uzio, M. Rivallan, D. Laurenti, and C. Geantet, "Understanding macromolecules formation from the catalytic hydroconversion of pyrolysis bio-oil model compounds," *Biomass and Bioenergy,* vol. 95, pp. 182-193, (2016).

[43] A. G. Gayubo, A. T. Aguayo, A. Atutxa, R. Aguado, M. Olazar, and J. Bilbao, "Transformation of oxygenate components of biomass pyrolysis oil on a HZSM-5 zeolite. II. Aldehydes, ketones, and acids," *Industrial & engineering chemistry research,* vol. 43, no. 11, pp. 2619-2626, (2004).

[44] Q. Almas, C. Sievers, and C. W. Jones, "Role of the mesopore generation method in structure, activity and stability of MFI catalysts in glycerol acetylation," *Applied Catalysis A: General,* vol. 571, pp. 107-117, (2019).

[45] G. Wu, N. Zhang, W. Dai, N. Guan, and L. Li, "Construction of Bifunctional Co/H-ZSM-5 Catalysts for the Hydrodeoxygenation of Stearic Acid to Diesel-Range Alkanes," *ChemSusChem,* vol. 11, no. 13, pp. 2179-2188, (2018).

[46] Z. Liu *et al.*, "Tailoring acidity of HZSM-5 nanoparticles for methyl bromide dehydrobromination by Al and Mg incorporation," *Nanoscale Research Letters,* vol. 9, no. 1, pp. 1-12, (2014).

[47] P. Iadrat and C. Wattanakit, "Bioethanol Upgrading to Renewable Monomers Using Hierarchical Zeolites: Catalyst Preparation, Characterization, and Catalytic Studies," *Catalysts,* vol. 11, no. 10, p. 1162, (2021).

[48] G. L. Woolery, G. H. Kuehl, H. C. Timken, A. W. Chester, and J. C. Vartuli, "On the nature of framework Brønsted and Lewis acid sites in ZSM-5," *Zeolites,* vol. 19, no. 4, pp. 288-296, (1997).

[49] V. Balasundram *et al.*, "Thermogravimetric catalytic pyrolysis and kinetic studies of coconut copra and rice husk for possible maximum production of pyrolysis oil," *Journal of cleaner production,* vol. 167, pp. 218-228, (2017).

[50] H. Yang, R. Yan, T. Chin, D. T. Liang, H. Chen, and C. Zheng, "Thermogravimetric analysis− Fourier transform infrared analysis of palm oil waste pyrolysis," *Energy & fuels,* vol. 18, no. 6, pp. 1814-1821, (2004).

[51] M. Amutio, G. Lopez, R. Aguado, M. Artetxe, J. Bilbao, and M. Olazar, "Kinetic study of lignocellulosic biomass oxidative pyrolysis," *Fuel,* vol. 95, pp. 305-311, (2012).

[52] M. Tauseef *et al.*, "Thermokinetics synergistic effects on co-pyrolysis of coal and rice husk blends for bioenergy production," *Fuel,* vol. 318, p. 123685, 2022/06/15/ (2022).

[53] A. Zaker, Z. Chen, and M. Zaheer-Uddin, "Catalytic pyrolysis of sewage sludge with HZSM5 and sludge-derived activated char: A comparative study using TGA-MS and artificial neural networks," *Journal of Environmental Chemical Engineering,* vol. 9, no. 5, p. 105891, (2021).

[54] Y. S. Kim, Y. S. Kim, and S. H. Kim, "Investigation of thermodynamic parameters in the thermal decomposition of plastic waste− waste lube oil compounds," *Environmental science & technology,* vol. 44, no. 13, pp. 5313-5317, (2010).

[55] M. Kumar, P. K. Mishra, and S. N. Upadhyay, "Thermal degradation of rice husk: effect of pre-treatment on kinetic and thermodynamic parameters," *Fuel*, vol. 268, p. 117164, (2020).

[56] S. Singh, J. P. Chakraborty, and M. K. Mondal, "Intrinsic kinetics, thermodynamic parameters and reaction mechanism of non-isothermal degradation of torrefied Acacia nilotica using isoconversional methods," *Fuel*, vol. 259, p. 116263, (2020).

[57] H. Li, S.-l. Niu, C.-m. Lu, and S.-q. Cheng, "Comparative evaluation of thermal degradation for biodiesels derived from various feedstocks through transesterification," *Energy Conversion and Management*, vol. 98, pp. 81-88, (2015).

[58] S. C. Turmanova, S. D. Genieva, A. S. Dimitrova, and L. T. Vlaev, "Non-isothermal degradation kinetics of filled with rise husk ash polypropene composites," *Express Polym Lett*, vol. 2, no. 2, pp. 133-146, (2008).

[59] M. Irfan *et al.*, "Assessing the energy dynamics of Pakistan: prospects of biomass energy," *Energy Reports*, vol. 6, pp. 80-93, (2020).

[60] L. Huang *et al.*, "Thermodynamics and kinetics parameters of co-combustion between sewage sludge and water hyacinth in CO2/O2 atmosphere as biomass to solid biofuel," *Bioresource Technology*, vol. 218, pp. 631-642, (2016).

[61] A. A. D. Maia and L. C. de Morais, "Kinetic parameters of red pepper waste as biomass to solid biofuel," *Bioresource technology*, vol. 204, pp. 157-163, (2016).

[62] Y. Xu and B. Chen, "Investigation of thermodynamic parameters in the pyrolysis conversion of biomass and manure to biochars using thermogravimetric analysis," *Bioresource technology*, vol. 146, pp. 485-493, (2013).